

# Journal of Materials Chemistry A

Accepted Manuscript



This is an *Accepted Manuscript*, which has been through the Royal Society of Chemistry peer review process and has been accepted for publication.

*Accepted Manuscripts* are published online shortly after acceptance, before technical editing, formatting and proof reading. Using this free service, authors can make their results available to the community, in citable form, before we publish the edited article. We will replace this *Accepted Manuscript* with the edited and formatted *Advance Article* as soon as it is available.

You can find more information about *Accepted Manuscripts* in the [Information for Authors](#).

Please note that technical editing may introduce minor changes to the text and/or graphics, which may alter content. The journal's standard [Terms & Conditions](#) and the [Ethical guidelines](#) still apply. In no event shall the Royal Society of Chemistry be held responsible for any errors or omissions in this *Accepted Manuscript* or any consequences arising from the use of any information it contains.

## ARTICLE

# Low Cost and Environment-benign Crack-blocking Structure for Long Life and High Power Si Electrodes in Lithium Ion Batteries

Cite this: DOI: 10.1039/x0xx00000x

Received 00th January 2012,  
Accepted 00th January 2012Min Ling<sup>a,b</sup>, Hui Zhao<sup>b</sup>, Xingcheng Xiao<sup>c</sup>, Feifei Shi<sup>b</sup>, Mingyan Wu<sup>b</sup>, Jingxia Qiu<sup>a</sup>,  
Sheng Li<sup>a</sup>, Xiangyun Song<sup>b</sup>, Gao Liu<sup>b\*</sup> and Shanqing Zhang<sup>a\*</sup>

DOI: 10.1039/x0xx00000x

www.rsc.org/

The high capacity Si (4200 mAh/g, Li<sub>4.4</sub>Si) commonly undergoes cracking and delamination due to drastic volume change (~300%) during lithiation/delithiation processes in lithium ion batteries (LIBs). In this work, abundant and sustainable natural polymer gum arabic (GA) and low cost polyacrylic acid (PAA) are used to fabricate Si anode with resilient, crack-blocking property. Esterification reaction between GA and PAA establishes a flexible network resulting in reinforced mechanical strength and enhanced coherent strength. Meanwhile, the water vapour resulted from the esterification reaction generates micron-sized pores which relieves the stress and blocks the formation and propagation of cracks. As a result of the crack-blocking effect, the resultant Si anodes present a superior volumetric capacity of 2890 Ah/L. In addition, charge-discharge cycling for more than 1000 cycles is achieved with Li insertion capacity limited to 1000 mAh/g at 1 C rate.

## Introduction

Lithium ion batteries (LIBs) are expanding their applications from conventional portable electronics to emerging large-scale energy storage devices, including hybrid electric vehicles (HEVs), pure electric vehicles (EVs) and smart electricity grids.<sup>1,2</sup> Hence, there is a critical demand for improving of the energy density of LIBs. To achieve high energy density batteries, engineering these materials (eg. Silicon) into cells has not been very successful through conventional binders (e.g. polyvinylidene fluoride). Moreover, the traditional electrode fabrication process commonly involves the use of toxic organic solvents, which has attracted public concerns from the environmental prospective. As a result, low cost and sustainable green high energy density electrode fabrication processes using natural binders have been attracting more and more attention.<sup>3</sup>

Silicon (Si) has been researched intensively as an alternative anode material for LIBs in last decade owing to its high theoretical gravimetric specific capacity of 4200 mAh/g (Li<sub>4.4</sub>Si), low lithiation/delithiation potential, the natural abundance of elemental Si, safety and environmental benignity.<sup>4</sup> However, Si-based anodes also face grand challenges due to ca. 300% volume expansion during lithiation/delithiation processes, which commonly pulverizes, cracks and breaks electrical contact between the Si particles with conductive additive and current collector, resulting in rapid capacity loss.<sup>5</sup> Recently, significant progress has been made through the synthesis of various nanostructured Si such as nanowires,<sup>6,7,8</sup> nano-fibers,<sup>9</sup> nanotubes,<sup>10</sup> nano-porous materials and Si/carbon nano-composites<sup>11-13</sup>. However, these methods are commonly sophisticated, time-consuming, high cost and not environmentally benign. Besides, new polymer binders other than traditional polyvinylidene fluoride (PVDF), including polyacrylic acid (PAA),<sup>14</sup> carboxyl-methyl cellulose (CMC),<sup>15</sup> crosslinking CMC and PAA,<sup>16</sup> sodium alginate,<sup>17</sup> mussel-inspired binder<sup>18</sup> and electronically conductive polymer binder<sup>19,20</sup> were proposed to resolve the problem and enhance the cycle life.<sup>21,22</sup> Although remarkable improvements in the electrochemical performance of Si-based anodes have been achieved, deformation of electrode due to the drastic volume change persists in varying extents. This is especially true for high Si loading electrode. This phenomenon was also observed in graphite based electrode after long-term cycling due to the gradual evolution and propagation of cracks in the electrode.<sup>23,24</sup>

In this work, a polymerization-induced crack-blocking polymer binder system, gum arabic (GA)-polyacrylic acid (PAA) composite, is designed for high energy density Si electrode. GA is a complex mixture of glycoproteins and polysaccharides. Glycoproteins are proteins that contain oligosaccharide chains covalently attached to polypeptide side-chains. Polysaccharides are long carbohydrate monosaccharide's units joined together by glycosidic bonds. A typical monosaccharide has the structure of H-(CHOH)<sub>x</sub>(C=O)-

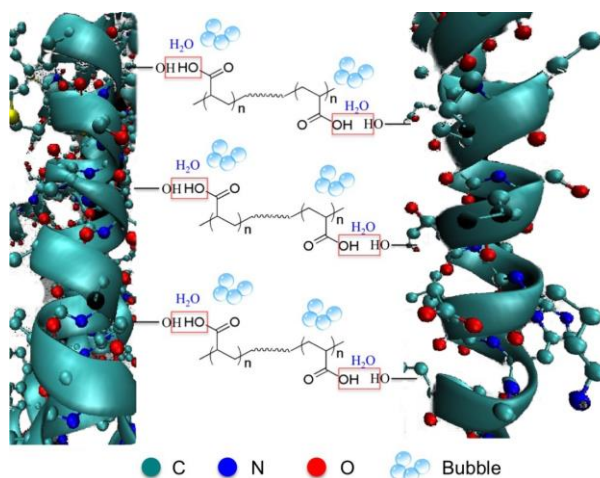


**Fig. 1** Schematic diagram of the polymeric reaction: the generation of water and formation of crack-blocking GA-PAA composite binder.

(CHOH)<sub>y</sub>-H, that is, an aldehyde or ketone with many hydroxyl groups, usually one on each carbon atom that is not part of the aldehyde or ketone functional group.<sup>25, 26</sup> The diversity of the oligosaccharides and protein structures create structure variation of the GA, making the hydroxide functional groups accessible to future function. PAA has gained popularity as a binder material for Si due to the rich carboxyl functional groups, and the ease of control of molecular weight through synthetic process.<sup>14</sup> A flexible polymer could have better capacity to tolerate the volume change and slow down the crack formation. The cracks in the composite electrode normally emerge at interfaces of the binder and particles when the volume of the particles changes.<sup>27-29</sup> Under continuous conditions stress (i.e., expansion of the active materials) the cracks propagate and grow.<sup>30-32</sup> Developing stress-relieving micron-pores in the crack propagation paths in the polymer binder can afford the crack damping and stopping function, leading to improved cycling performance.

The rich hydroxyl and carboxyl functional groups along with the flexibility of the binders improve the interface adhesion.<sup>33-35</sup> Between the hydroxyl groups on GA and carboxyl groups on PAA polymer, condensation reaction is triggered at 150 °C to form ester bonds and produce flexible networks under vacuum condition in this work, as shown in Fig. 1.<sup>16</sup> The detailed chemical composition is included in Fig. S1. The esterification and dehydration process lead to the formation of water that subsequently escape from the polymer. The formation and evaporation of the water from the polymer create submicron-sized pores within the resultant composite.

It is well established that the pores in the crack propagation path could effectively relieve mechanical stress and stop crack-growing in metal, glass and ceramic based materials. In order to utilize this phenomenon to resolve the crack propagation, pores are created deliberately in the cracking object, for example holes are commonly drilled in the wind screen glass to avoid further cracking. (Fig. S2a, b).<sup>36, 37</sup> Micron-pores can be created by chemical reaction in the electrode to mimic the stress-relieving function of the drilled holes as in the metal and glass materials. Without the pores, as showed in Fig. S2c and d, the crack will extended much longer distance in the electrode. The micron-pores showed in Fig. S2e are created via water evaporation from the esterification reaction between the GA and PAA. More SEM images of the micron-pores originated from the condensation reaction are detailed in Fig. S3.

## Results and discussion

The thermal stabilities of GA, PAA, GA/PAA mixture (refer to the mixture without esterification reaction) and GA-PAA composite (refer to the composite generated by the esterification reaction, detailed in supplementary information) polymers are preliminarily examined using thermal gravimetric analysis (TGA). The sample is firstly kept at 80 °C for 60 min to remove the adsorbed water and then carried out up to 800 °C to perform a carbonization process of the polymers. Fig. S4a shows that the carbonization initiates at ca. 260 °C and ca. 220 °C for GA and PAA, respectively. It can be observed easily that the weight loss for the GA-PAA composite (after esterification) is the smallest compared with the GA, PAA, and GA/PAA mixture (before esterification). Overall, Fig. S4a suggests that the GA PAA composite can afford a wide working temperature range (up to 170 °C), including the typical working temperature range (0-40 °C) of LIBs.

The electrochemical behavior of the binders is evaluated by cyclic voltammetry (CV) in a potential range from 0.01 V to 1.00 V at a scan rate of 0.2 mV/s (Fig. S4b, c). The reversible CV profile confirmed that GA, PAA and GA-PAA composite binders are electrochemically stable in the Si anode working voltage range (i.e., 0.01-1.00 V). Adhesion capability of binders between the active materials and current collector is of primary requirement for applications in LIBs. Low adhesion in electrodes leads to the delamination of active materials from the current collector and ultimately causes significant capacity loss during charge/discharge cycles.<sup>38</sup> As shown in Fig. S4d, both laminates (the GA-PAA composite and GA/PAA mixture) can persist on the current collector with no crack or delamination observed through the entire adhesion test up to 1.5-2.0 pounds peel force. In spite of the decrease of adhesion functional groups (such as hydroxyl on GA and carboxyl on PAA) due to the esterification reaction between the GA and PAA binder, the binding force of the GA-PAA composite does not decline but increase. This can be explained by the crosslinking function of the GA and PAA polymers to form robust network structure.<sup>18</sup> The enhanced binding force bestows the GA-PAA composite a promising binder for high Si loading electrodes.

Although Si anode materials have high theoretical capacity, one of the key obstacles for the industrialization of Si anode is the insufficient areal capacity, i.e., the energy density.<sup>39-41</sup> The Si mass loadings nowadays are typically ca. 0.2-0.3 mg/cm<sup>2</sup>,<sup>16, 17, 20, 42</sup> which is below the commercialization standards. Recently, a pomegranate-inspired nanoscale material design and PAA-PVA binder system were developed in order to achieve high volumetric capacity when the areal capacity is increased to the level of commercial LIBs.<sup>43, 44</sup> To achieve the higher energy density and specific capacity, the crack-blocking GA-PAA composite binder is applied to tackle this problem from electrode design aspect. With the increased mass loading to 1.0 mg/cm<sup>2</sup>, as shown in Fig. 2, the typical discharge and charge profiles at current densities of C/10 (420 mA/g) and C/5 (840 mA/g) are performed. The first discharge and charge capacities are found to be 4123 mAh/g and 3816 mAh/g, respectively, with an initial Coulombic efficiency of 92.55 %. The irreversible capacity loss in the first cycle is due to the solid electrolyte interphase (SEI) formation (Fig. S5, slope from 1.0 V to 0.3 V), during this process the electrolyte reductively decomposed to form a passivation layer, which prevents further electrolyte decomposition and allows reversible lithiation/delithiation of the Si active materials. The SEI component formation is facilitated by the fluoroethylene carbonate (FEC), an effective electrolyte additive for Si-based lithium-ion battery.<sup>45, 46</sup> After the first few cycles, the Coulombic efficiency rapidly increased to above 99 %. It remained stable throughout the cycles, indicating that the high loading Si anode is stable and the cell showed excellent reversible cycling after the SEI formation.

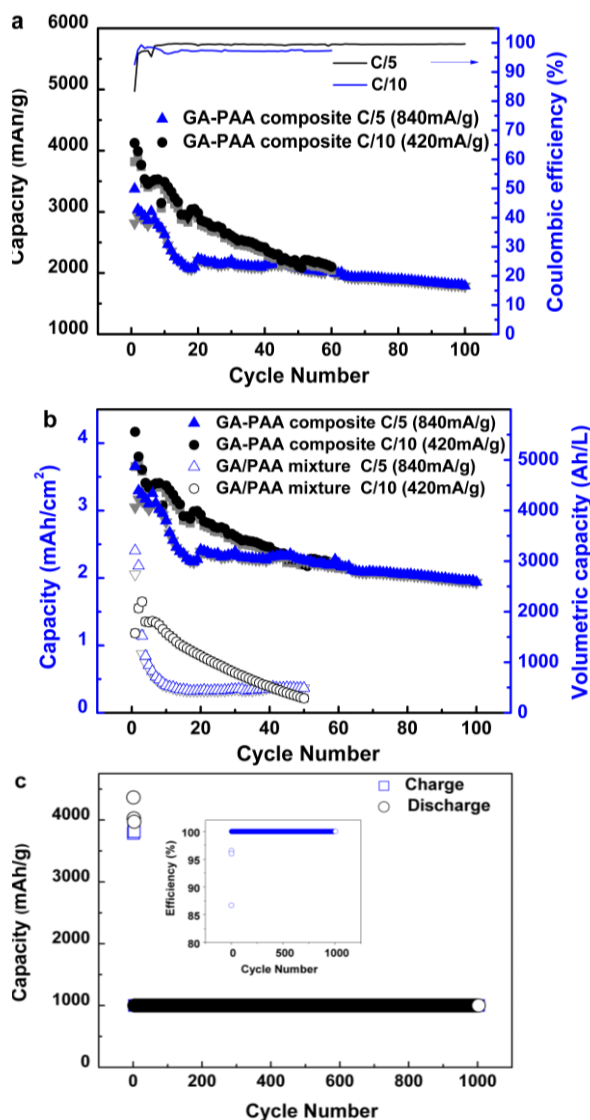


**Fig. 2.** (a, b) Reversible Li-extraction capacity of the Si electrodes based on GA and GA-PAA composite binder collected at the C/10 (420 mA/g) and C/5 rate (840 mA/g). (c) Reversible Li-extraction capacity and Coulombic efficiency of the Si electrodes for Li insertion level fixed to 1000 mAh/g Si (Ah, ampere hour) at 1C rate (4200 mA/g) over the potential window of 0.01-1 V (versus  $\text{Li}/\text{Li}^+$ ) (Si:C:binder = 2:1:1, wt%).

It should be noted that high specific capacity normalized by the weight of the active materials with low areal loading actually means low energy density. The crack-blocking effect help achieve remarkable high loading performance. The first cycle reversible volumetric capacities for high loading GA-PAA composite binder based electrode are 5478 Ah/L and 4573 Ah/L, respectively, for 0.1 C (420 mA/g) and 0.2 C (840 mA/g). The volumetric capacity can be increased to more than 5 times compared to the GA/PAA mixture binder based electrode (Fig. 2b), much higher than the density of the current commercialized LIBs. After 100 cycles at 0.2 C, GA-PAA electrode can preserve 63.3 % of the original capacity (2898 Ah/L). The capacity retention capability of the electrode is quite remarkable considering the 5 times increase of mass loading. The energy density of the electrode is ca. 5 times that of graphite electrode (ca. 600

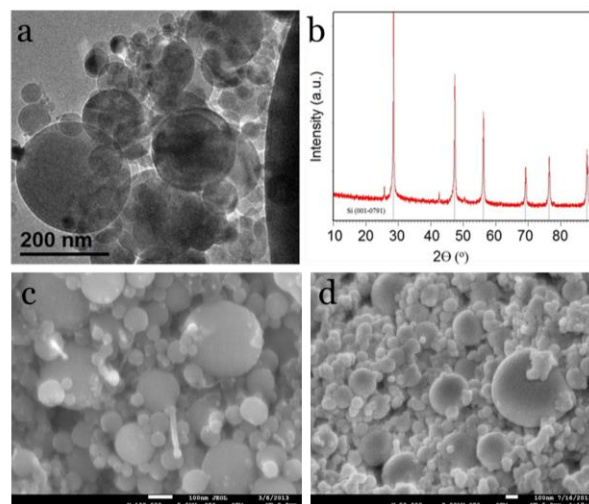


**Figure 3** (a) TEM image of Si before fabrication. (b) XRD diffraction of Si. Microstructure of the Si electrodes with (c) GA/PAA mixture and (d) GA-PAA composite binder (Si:C:binder = 2:1:1, wt %).

Ah/L) even after 100 cycles.<sup>50</sup> The fact that theoretical volumetric capacity of the 7.5  $\mu\text{m}$  thickness of the GA-PAA composite laminate is ca. 5580 Ah/L, suggests that almost all the Si in the thick electrode is active and that the crack-blocking micron-pores formed due to esterification in the electrodes play a critical role for the performance of thicker electrodes. In comparison, the pure PAA binder based Si electrodes deliver 1.95 mAh/cm<sup>2</sup> at the first cycle, which is significantly lower than that of the GA-PAA composite sample. Furthermore, it could only preserve ca. 10% after 100 cycles (see Fig. S6).

The optimization of Si anodes can be achieved from two pathways, i.e., the application of novel functional binders as shown in recent works<sup>14, 15, 18, 34, 35, 48, 49</sup> in Table 1 and modification and fabrication of Si electrode with nanostructure and morphology as shown in Table 2<sup>43, 51, 10, 52-56</sup>. The modification of Si materials commonly involves high cost, time-consuming and sophisticate advanced synthesis process. In contrast, application of the new

**Table 1.** The comparison of the GA-PAA binder system and other recent reported binder system in cyclability and volumetric energy density of LIBs.

Materials	Cyclability	Energy Density
GA-PAA (This work)	1000 mAh/g for 1000 cycles ( <b>1C</b> )	ca. 2890 Ah/L ( <b>0.2C</b> )
PEFM (2013) <sup>47</sup>	3100 mAh/g for 50 cycles ( <b>0.3C</b> )	ca. 1200 Ah/L ( <b>0.1C</b> )
Si-Alg-C (2013) <sup>18</sup>	900 mAh/g for 150 cycles ( <b>1C</b> )	N/A
c-PAA-CMC (2012) <sup>34</sup>	1800 mAh/g for 100 cycles ( <b>0.5C</b> )	N/A
PFFOMB (2011) <sup>48</sup>	2300 mAh/g for 650 cycles ( <b>0.1C</b> )	N/A
Alginate (2011) <sup>35</sup>	1800mAh/g for 100 cycles ( <b>1C</b> )	ca. 300 Ah/L ( <b>1C</b> )
Scaffold CMC-C/Nano Si (2010) <sup>49</sup>	1800 mAh/g for 150 cycles ( <b>0.05C</b> )	N/A
PAA (2010) <sup>14</sup>	2000 mAh/g for 100 cycles ( <b>0.5C</b> )	N/A

Table 2. The comparison of the GA-PAA binder based Si anode and the modified Si anodes in cyclability and volumetric energy density of LIBs.

GA-PAA (This work)	1000 mAh/g for 1000 cycles (1C)	ca. 2890 Ah/L (0.2C)
Pomegranate inspired Si (2014) <sup>43</sup>	1300 mAh/g for 1000 cycles (0.5C)	ca. 1270 Ah/L (ca. 0.07 C)
Nano-Micro composite Si (2013) <sup>51</sup>	2800 mAh/g for 30 cycles (0.5C)	ca. 600 Ah/L (0.1C)
Si hollow nanosphere (2011) <sup>52</sup>	1800 mAh/g for 700 cycles (0.5C)	N/A
Si nanotube (2010) <sup>53</sup>	2500 mAh/g for 50 cycles (0.2C)	N/A
Core-Shell Si nanowire <sup>54</sup>	1000 mAh/g for 100 cycles (0.2C)	N/A
3D porous Si (2008) <sup>55</sup>	2700 mAh/g for 100 cycles (0.2C)	N/A
Carbon Coated Si (2006) <sup>56</sup>	1800 mAh/g for 20 cycles (0.03C)	N/A

binder is generally economical, simple, scalable and generic if the binders are at low cost. Nevertheless, as shown in Table 1, the performance of the as-prepared GA-PAA is among the best of the Si electrodes using new binders in terms of cyclability and volumetric energy density. In comparison with these binders in Table 1, the GA-PAA binding process has additional merits of environmental sustainability besides the advantages of these binders. In particular, charge-discharge capacity of our Si electrode has been stabilized at 1000 mAh/g at the current density of 4200 mA/g for more than 1000 cycles (see Fig. 2c). The Si electrode with GA-PAA binder also shows superior performance to the modified nanostructured Si electrodes in Table 2. The outstanding stability and volumetric capacity achieved suggests that the GA-PAA process is a generic promising technology for high energy density LIBs applications such as smart electricity grid and secondary batteries for green energy such as wind energy and solar energy.

Fig. 3 shows the details of the incorporated Si anode materials. The Si particle size distribution is ca. 200 nm diameters, with some particles reaching micron scale. All the X-ray diffraction (XRD) peaks correspond well with standard crystallographic data (International Centre for Diffraction Data (ICDD) File No. 001-0791). The scanning electron microscopy (SEM) of the Si electrode based on GA/PAA mixture (Fig. 3c) and GA-PAA composite binder (Fig. 3d) are shown respectively. The energy dispersive X-ray spectroscopy (EDS) in Fig. S7 shows the uniformly distribution of Si particles in the electrodes. Interestingly, it is observed that the GA-PAA composite electrode after the esterification has more compact structure compared with other electrodes that can result in higher energy density of the LIBs.

Li-ion transportation in the binder system is critical for achieving the full capacity for the Si anode materials with high specific capacity. The electrolyte uptake is important for allowing facile Li-ion transportation through the polymer binder to the active materials. In the crack-blocking binder system, after the entrant of PAA, the electrolyte uptake is accounting for ca. 25 wt% of its final weight, which is higher than the GA/PAA mixture (17.2 wt%) and PVDF (11.5 wt%) swelling in the electrolyte (Fig. S8). It is interesting to note that the value of GA/PAA mixture is between that of GA (19.5 wt%) and PAA (14.6 wt%) polymer; Nevertheless, the

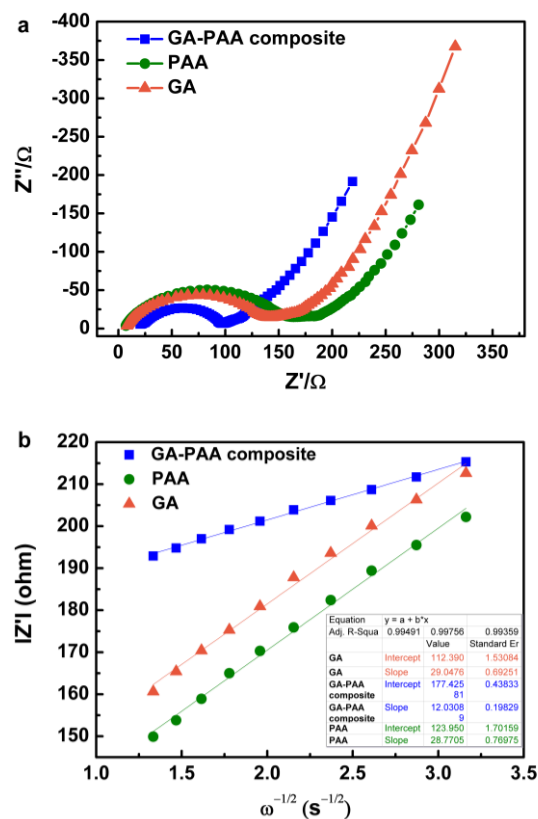


Figure 4 (a) EIS spectra of the GA-PAA composite, GA and PAA samples between 0.1 Hz and 100 kHz. (b) The relationship between  $Z'$  and  $\omega^{-0.5}$  at low frequency.

uptake amount for GA-PAA composite surpasses all the precursors and GA/PAA mixture polymer, which can be ascribed to the micropores in the crack-blocking structure. The high electrolyte uptake is beneficial to the high lithium ion diffusion efficiency and subsequently facilitates the high capacity and power of the Si electrode.<sup>47</sup> The electrochemical impedance spectra (EIS) of the electrodes with different binders are measured as shown in Fig. 4. The plot includes the real component of impedance on the horizontal axis ( $Z'$ ), and the imaginary component of the impedance on the vertical axis ( $Z''$ ). It is well-established that the ohmic resistance ( $R_s$ ) through the multilayer surface and the charge transfer resistance ( $R_{ct}$ ) are represented by intersection on  $x$  axis and the diameters of the semicircles respectively in the profiles.<sup>57</sup> As shown in Fig. 4a, the  $R_{ct}$  of Ga-PAA composite sample is significantly lower than that of PAA and GA samples ascribed to the as generated pores in the electrode. The parameters of impedance spectra is simulated and fitted with an equivalent circuit by ZView™ software. The Warburg coefficient  $\sigma_w$  can be calculated by the Equation (1):

$$|Z'| = R_s + R_{ct} + \sigma_w \omega^{-0.5} \quad (1)$$

In addition, the plot of  $Z'$  vs. the reciprocal square roots of the lower angular frequencies is shown in Fig 4b. The slope of the fitted line is the Warburg coefficient  $\sigma_w$ . The calculated value of  $\sigma_w$  for GA-PAA composite, GA and PAA based binder is 12.0, 29.0 and 28.7, respectively (Fig. 4b). Because diffusion coefficient of Lithium ion is inversely proportional to warburg coefficient  $\sigma_w$  as shown in Equation (2)<sup>58</sup>:

$$D_{Li} = \frac{1}{V_M S F A \sigma^2} \quad (2)$$

Where  $V_M$  is the Silicon molar volume,  $S$  is the contact area between electrolyte and sample,  $F$  is the Faraday constant,  $\sigma$  are the warburg coefficient. The GA-PAA composite electrode has the highest  $D_{Li}$  compared with the pure GA and PAA samples.<sup>59</sup>

Fourier Transform Infrared Spectroscopy (FTIR) together with TGA, is used to examine the extend of the esterification reaction between GA and PAA. The FTIR spectra in Fig. S9a show the different functional groups of GA and the functional groups change before and after the condensation reaction. The peak at ca. 3500  $\text{cm}^{-1}$  can be ascribed to the hydroxyl groups while the peaks at ca. 1150  $\text{cm}^{-1}$  and 1250  $\text{cm}^{-1}$  demonstrate that the esterification occurred between the PAA (carboxylic groups) and GA (hydroxyl groups), leading to the polymeric network that encapsulate the Si nanoparticles and carbon black together and subsequently benefits the cycle stability. Besides, the crack-blocking structure restructured after the esterification reaction is the main factor that contributes to the high loading electrode capacity.<sup>60</sup>

Hence, we further keep the temperature stable at 150 °C for 1 hour to quantify the weight of water generated by the esterification reaction. The curves in Fig. S9b and c show that there is ca. 7.6 wt% adsorbed water removed at 80 °C for 1 hour. The stable plateau between 80 °C and 130 °C indicates the absolute removal of the adsorbed water. Then a further weight loss of ca. 3.2 wt% from 130 °C to 150 °C (Stabilized @ 150 °C for 1 h) reveals removal of water from condensation between GA and PAA. Hence, the esterification degree can be calculated as ca. 27 wt% according to the 3.2 wt% weight loss (See Fig. S9c). The BET analysis has been conducted and the BET adsorption and desorption profiles are inserted in the Supplementary Information as Fig. S10. The  $N_2$  adsorption and desorption isotherms at 77 K in Fig. S10 suggest that the surface area of the GA-PAA composite is ca. 60.5  $\text{m}^2/\text{g}$ .

The crack blocking function can further stable the electrode even when cracks are initiated. This improvement in terms of mechanical properties of the electrode laminates can be visually confirmed via scratch tests. The morphology of the GA-PAA composite based electrodes after a scratch has shown a drastic difference under SEM (Fig. S11). The scratch track of the GA-PAA composite sample is relatively smooth and dense, with a small number of narrow cracks on the scratched surface. This demonstrates that the crack-blocking surface is stronger and more resilient to stress, than the GA electrode surface when the identical scratch force is applied. Moreover, the micropores play a role in stopping the crack propagation even when the crack is initiated.

## Conclusions

High areal Si loading anodes with high volumetric capacity for LIBs are successfully assembled via a simple *in situ* esterification process through water-based natural polymer GA and PAA at 150 °C under vacuum. The esterification reaction between hydroxyl groups in GA and carboxylic acid groups in PAA provides reinforced mechanical strength and lithium diffusion capability. The micron-sized pores formed during the process block the crack formation and propagation by relieving the stress of the electrode due to the dramatic volume change of Si particles during lithiation/delithiation processes. The excellent thermal, electrochemical and mechanical stability of the GA-PAA composite facilitates high volumetric capacity and long-term cycle performance that demonstrate promising potential for industrial application.

## Acknowledgements

This work is supported by the Australia Research Council and by the Assistant Secretary for Energy Efficiency, Office of Vehicle Technologies of the U.S. Department of Energy (U.S. DOE) under contract no. DE-AC02-05CH11231 and the Batteries for Advanced Transportation Technologies (BATT) Program at Lawrence Berkeley National Laboratory.

## Notes and references

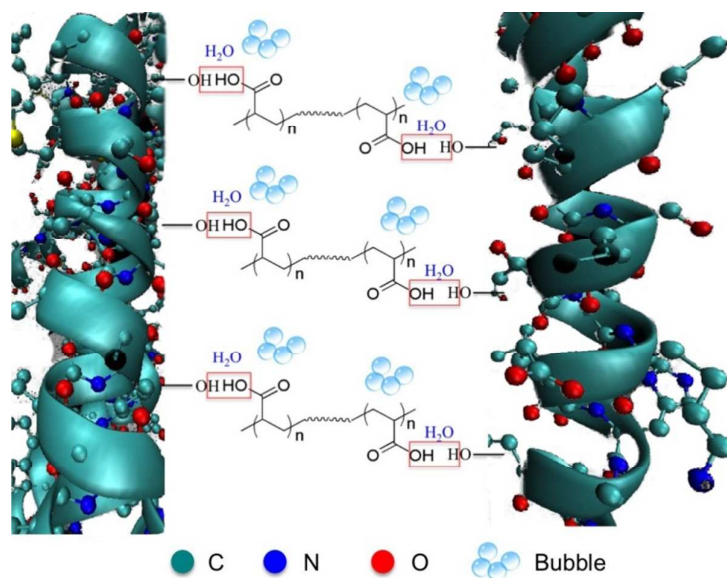
<sup>a</sup>Center for Clean Environment and Energy, Environmental Futures Research Institute and Griffith School of Environment, Gold Coast Campus, Griffith University, Australia.

<sup>b</sup>Environmental Energy Technologies Division, Lawrence Berkeley National Laboratory, Berkeley, California, USA.

Electronic Supplementary Information (ESI) available: [details of any supplementary information available should be included here].

1. M. Armand and J. M. Tarascon, *Nature*, 2008, **451**, 652-657.
2. M. M. Thackeray, C. Wolverton and E. D. Isaacs, *Energy Environ. Sci.*, 2012, **5**, 7854-7863.
3. J. B. Goodenough and Y. Kim, *Chem. Mater.*, 2010, **22**, 587-603.
4. A. S. Arico, P. Bruce, B. Scrosati, J. M. Tarascon and W. Van Schalkwijk, *Nat. Mater.*, 2005, **4**, 366-377.
5. U. Kasavajjula, C. S. Wang and A. J. Appleby, *J. Power Sources*, 2007, **163**, 1003-1039.
6. L. Hu, H. Wu, S. S. Hong, L. Cui, J. R. McDonough, S. Bohy and Y. Cui, *Chem. Commun.*, 2011, **47**, 367-369.
7. K. Kang, K. Song, H. Heo, S. Yoo, G.-S. Kim, G. Lee, Y.-M. Kang and M.-H. Jo, *Chem. Sci.*, 2011, **2**, 1090-1093.
8. W. Ren, C. Wang, L. Lu, D. Li, C. Cheng and J. Liu, *J. Mater. Chem. A*, 2013, **1**, 13433-13438.
9. L.-F. Cui, Y. Yang, C.-M. Hsu and Y. Cui, *Nano Lett.*, 2009, **9**, 3370-3374.
10. M.-H. Park, M. G. Kim, J. Joo, K. Kim, J. Kim, S. Ahn, Y. Cui and J. Cho, *Nano Lett.*, 2009, **9**, 3844-3847.
11. J. Song, S. Chen, M. Zhou, T. Xu, D. Lv, M. L. Gordin, T. Long, M. Melnyk and D. Wang, *J. Mater. Chem. A*, 2014, **2**, 1257-1262.
12. R. Yi, F. Dai, M. L. Gordin, S. Chen and D. Wang, *Adv. Energy Mater.*, 2013, **3**, 295-300.
13. R. Yi, J. Zai, F. Dai, M. L. Gordin and D. Wang, *Nano Energy*, 2014, **6**, 211-218.
14. A. Magasinski, B. Zdyrko, I. Kovalenko, B. Hertzberg, R. Burtovyy, C. F. Huebner, T. F. Fuller, I. Luzinov and G. Yushin, *ACS Appl. Mater. Inter.*, 2010, **2**, 3004-3010.
15. J. Li, R. B. Lewis and J. R. Dahn, *Electrochem. Solid-State Lett.*, 2007, **10**, A17-A20.
16. B. Koo, H. Kim, Y. Cho, K. T. Lee, N.-S. Choi and J. Cho, *Angew. Chem., Int. Ed.*, 2012, **51**, 8762-8767.
17. I. Kovalenko, B. Zdyrko, A. Magasinski, B. Hertzberg, Z. Milicev, R. Burtovyy, I. Luzinov and G. Yushin, *Science*, 2011, **334**, 75-79.
18. M. H. Ryou, J. Kim, I. Lee, S. Kim, Y. K. Jeong, S. Hong, J. H. Ryu, T. S. Kim, J. K. Park, H. Lee and J. W. Choi, *Adv. Mater.*, 2013, **25**, 1571-1576.
19. M. Y. Wu, X. C. Xiao, N. Vukmirovic, S. D. Xun, P. K. Das, X. Y. Song, P. Olalde-Velasco, D. D. Wang, A. Z. Weber, L. W. Wang, V. S. Battaglia, W. L. Yang and G. Liu, *J. Am. Chem. Soc.*, 2013, **135**, 12048-12056.
20. G. Liu, S. D. Xun, N. Vukmirovic, X. Y. Song, P. Olalde-Velasco, H. H. Zheng, V. S. Battaglia, L. W. Wang and W. L. Yang, *Adv. Mater.*, 2011, **23**, 4679-+.
21. A. Magasinski, P. Dixon, B. Hertzberg, A. Kvit, J. Ayala and G. Yushin, *Nat. Mater.*, 2010, **9**, 353-358.
22. J. Guo and C. Wang, *Chem. Commun.*, 2010, **46**, 1428-1430.
23. S. Bhattacharya, A. R. Riahi and A. T. Alpas, *J. Power Sources*, 2011, **196**, 8719-8727.
24. R. Grantab and V. B. Shenoy, *J. Electrochem. Soc.*, 2011, **158**, A948-A954.
25. N. A. Ademoh, *Int. J. Phys. Sci.*, 2010, **5**, 557-563.
26. A. P. I. Popoola, *J. Sci. Ind. Res.*, 2011, **70**, 1029-1032.
27. E. K. Rahani and V. B. Shenoy, *J. Electrochem. Soc.*, 2013, **160**, A1153-A1162.

28. H. H. Zheng, L. Zhang, G. Liu, X. Y. Song and V. S. Battaglia, *J. Power Sources*, 2012, **217**, 530-537.
29. J. H. Kim, S. C. Woo, M. S. Park, K. J. Kim, T. Yim, J. S. Kim and Y. J. Kim, *J. Power Sources*, 2013, **229**, 190-197.
30. C. Makabe, A. Murdani, K. Kuniyoshi, Y. Irei and A. Saimoto, *Eng. Fail. Anal.*, 2009, **16**, 475-483.
31. C. S. Shin, C. M. Wang and P. S. Song, *Int. J. Fatigue.*, 1996, **18**, 535-546.
32. N. Vulic, S. Jecic and V. Grubisic, *Int. J. Fatigue.*, 1997, **19**, 283-291.
33. M. Murase, N. Yabuuchi, Z.-J. Han, J.-Y. Son, Y.-T. Cui, H. Oji and S. Komaba, *Chemsuschem*, 2012, **5**, 2307-2311.
34. K. Bonjae, K. Hyunjung, C. Younghyun, L. Kyu Tae, C. Nam-Soon and C. Jaephil, *Angew. Chem., Int. Ed.*, 2012, **51**, 8762-8767.
35. I. Kovalenko, B. Zdyrko, A. Magasinski, B. Hertzberg, Z. Milicev, R. Burtovyy, I. Luzinov and G. Yushin, *Science*, 2011, **334**, 75-79.
36. A. Murdani, C. Makabe, A. Saimoto and R. Kondou, *Eng. Fail. Anal.*, 2008, **15**, 302-310.
37. P. S. Song and Y. L. Shieh, *Int. J. Fatigue.*, 2004, **26**, 1333-1339.
38. J. Chen, J. Liu, Y. Qi, T. Sun and X. Li, *J. Electrochem. Soc.*, 2013, **160**, A1502-A1509.
39. M. Ge, X. Fang, J. Rong and C. Zhou, *Nanotechnol.*, 2013, **24**.
40. M. L. Terranova, S. Orlanducci, E. Tamburri, V. Guglielmotti and M. Rossi, *J. Power Sources*, 2013, **246**, 167-177.
41. S. D. Xun, B. Xiang, A. Minor, V. Battaglia and G. Liu, *J. Electrochem. Soc.*, 2013, **160**, A1380-A1383.
42. H. Wu, G. H. Yu, L. J. Pan, N. A. Liu, M. T. McDowell, Z. A. Bao and Y. Cui, *Nat. Commun.*, 2013, **4**.
43. N. Liu, Z. Lu, J. Zhao, M. T. McDowell, H.-W. Lee, W. Zhao and Y. Cui, *Nat. Nanotechnol.*, 2014, **9**, 187-192.
44. J. Song, M. Zhou, R. Yi, T. Xu, M. L. Gordin, D. Tang, Z. Yu, M. Regula and D. Wang, *Adv. Funct. Mater.*, 2014, **24**, 5904-5910.
45. H. Nakai, T. Kubota, A. Kita and A. Kawashima, *J. Electrochem. Soc.*, 2011, **158**, A798-A801.
46. M. Y. Nie, D. P. Abraham, Y. J. Chen, A. Bose and B. L. Lucht, *J. Phys. Chem. C*, 2013, **117**, 13403-13412.
47. M. Wu, X. Xiao, N. Vukmirovic, S. Xun, P. K. Das, X. Song, P. Olalde-Velasco, D. Wang, A. Z. Weber, L.-W. Wang, V. S. Battaglia, W. Yang and G. Liu, *J. Am. Chem. Soc.*, 2013, **135**, 12048-12056.
48. G. Liu, S. Xun, N. Vukmirovic, X. Song, P. Olalde-Velasco, H. Zheng, V. S. Battaglia, L. Wang and W. Yang, *Adv Mater*, 2011, **23**, 4679-4683.
49. J. C. Guo and C. S. Wang, *Chem. Commun.*, 2010, **46**, 1428-1430.
50. M. Endo, C. Kim, K. Nishimura, T. Fujino and K. Miyashita, *Carbon*, 2000, **38**, 183-197.
51. M. Wu, J. E. C. Sabisch, X. Song, A. M. Minor, V. S. Battaglia and G. Liu, *Nano Lett.*, 2013, **13**, 5397-5402.
52. Y. Yao, M. T. McDowell, I. Ryu, H. Wu, N. Liu, L. Hu, W. D. Nix and Y. Cui, *Nano Lett.*, 2011, **11**, 2949-2954.
53. T. Song, J. Xia, J.-H. Lee, D. H. Lee, M.-S. Kwon, J.-M. Choi, J. Wu, S. K. Doo, H. Chang, W. Il Park, D. S. Zang, H. Kim, Y. Huang, K.-C. Hwang, J. A. Rogers and U. Paik, *Nano Lett.*, 2010, **10**, 1710-1716.
54. L.-F. Cui, R. Ruffo, C. K. Chan, H. Peng and Y. Cui, *Nano Lett.*, 2009, **9**, 491-495.
55. H. Kim, B. Han, J. Choo and J. Cho, *Angew. Chem., Int. Ed.*, 2008, **47**, 10151-10154.
56. S.-H. Ng, J. Wang, D. Wexler, K. Konstantinov, Z.-P. Guo and H.-K. Liu, *Angew. Chem., Int. Ed.*, 2006, **45**, 6896-6899.
57. P. Yu, B. N. Popov, J. A. Ritter and R. E. White, *J. Electrochem. Soc.*, 1999, **146**, 8-14.
58. N. Ding, J. Xu, Y. X. Yao, G. Wegner, X. Fang, C. H. Chen and I. Lieberwirth, *Solid State Ionics*, 2009, **180**, 222-225.
59. P. P. Prossini, M. Lisi, D. Zane and M. Pasquali, *Solid State Ionics*, 2002, **148**, 45-51.
60. J. S. Bridel, T. Azais, M. Morcrette, J. M. Tarascon and D. Larcher, *Chem. Mater.*, 2010, **22**, 1229-1241.



A graphical illustration of the gum arabic (GA) and polyacrylic acid (PAA) composite binder.